Geophysical Research Letters

RESEARCH LETTER
10.1029/2024GL112038

Turbulent Energy Conversion Associated With Kinetic Microinstabilities in Earth's Magnetosheath

Harry C. Lewis[1], Julia E. Stawarz[2], Lorenzo Matteini[1], Luca Franci[2], Kristopher G. Klein[3], Robert T. Wicks[2], Chadi S. Salem[4], Timothy S. Horbury[1], and Joseph H. Wang[1]

[1]Department of Physics, Imperial College London, London, UK, [2]Department of Mathematics, Physics and Electrical Engineering, Northumbria University, Newcastle Upon Tyne, UK, [3]Lunar and Planetary Laboratory and Department of Planetary Sciences, University of Arizona, Tucson, AZ, USA, [4]Space Sciences Laboratory, University of California, Berkeley, CA, USA

Key Points:

- We explore the interplay between turbulent fluctuations and kinetic microinstabilities using MMS in Earth's magnetosheath
- We measure enhanced energy conversion when plasma is susceptible to electron and ion instabilities
- Unstable periods are scarce yet play an important role in regulating the thermodynamics of the plasma

Supporting Information:

Supporting Information may be found in the online version of this article.

Correspondence to:

H. C. Lewis,
h.lewis21@imperial.ac.uk

Citation:

Lewis, H. C., Stawarz, J. E., Matteini, L., Franci, L., Klein, K. G., Wicks, R. T., et al. (2024). Turbulent energy conversion associated with kinetic microinstabilities in Earth's magnetosheath. *Geophysical Research Letters*, *51*, e2024GL112038. https://doi.org/10.1029/2024GL112038

Received 16 AUG 2024
Accepted 18 NOV 2024

© 2024. The Author(s).
This is an open access article under the terms of the Creative Commons Attribution License, which permits use, distribution and reproduction in any medium, provided the original work is properly cited.

Abstract Plasma in Earth's magnetosheath rarely experiences interparticle collisions, so kinetic microinstabilities are thought to contribute to regulating the plasma thermodynamics. Instabilities excite waves and redistribute free energy in velocity space, reducing free energy in the velocity distribution function (VDF). Using 24 hr of data spread over 163 intervals of in situ magnetosheath observations by Magnetospheric Multiscale (MMS), we investigate signatures of energy conversion where the turbulent dynamics have locally distorted the VDFs into non-Maxwellian shapes, in the context of electron and ion temperature anisotropy driven instabilities. We find enhanced average energy conversion into the particles along instability boundaries, suggesting turbulence plays a role in redistributing free energy. In so doing, we quantify the energetics associated with unstable conditions for both species. This work provides insight into the open question of how specific plasma processes couple into the turbulent dynamics, ultimately leading to energy dissipation and particle energization in collisionless plasmas.

Plain Language Summary In the region of disturbed flow ahead of Earth's protective magnetic field, charged particles rarely experience collisions. As such, traditional mechanisms that control how energy is distributed between electromagnetic, bulk flow, and thermal energy are replaced by kinetic processes which couple the particles and electromagnetic fields. The phenomenon linking injection of energy at large scales to the heating of particles at small scales is turbulence, and it is unknown exactly how this process operates in a medium which lacks collisions. Our work investigates energy transfer related to turbulence in the context of kinetic processes under collisionless conditions, using satellite measurements to unravel how the average properties of energy conversion are altered when these processes—known as instabilities—are acting. We find that extra energy is imparted from the fields into the particles during periods when the turbulent fluctuations drive the medium toward a state that is susceptible to instabilities, highlighting that turbulence is playing a role in how these processes are initiated. Despite accounting for a small portion of the observed measurements, the work demonstrates such instabilities are playing an active role in regulating how different types of energy are distributed in turbulent collisionless plasmas.

1. Introduction

Plasma turbulence is the predominant process by which fluctuation energy is transferred from injection at large scales to dissipation at microphysical scales. This phenomenon is known as the turbulent cascade and operates in a wide range of astrophysical plasma environments (Galtier, 2018; Matthaeus & Velli, 2011; Stepanova et al., 2022), such as (but not limited to) planetary magnetospheres and ionospheres (Guio & Pécseli, 2021; Saur, 2021), stellar coronae (Cranmer et al., 2015; Zank et al., 2021), stellar winds (Adhikari et al., 2021; Bruno & Carbone, 2013; Carbone, 2012; Verscharen et al., 2019), the interstellar medium (Fraternale et al., 2022; Linsky et al., 2022), and beyond (Evoli & Ferrara, 2011; Ruszkowski & Pfrommer, 2023; Subramanian et al., 2006). Despite decades of intensive research, the nature of the kinetic-scale interactions which mediate dissipation in collisionless space plasmas are still poorly understood (e.g., Alexandrova et al., 2013; Chen, 2016; Kiyani et al., 2015; Marino & Sorriso-Valvo, 2023; Matthaeus, 2021; Sahraoui et al., 2020; Schekochihin, 2022; Smith & Vasquez, 2021).

The magnetosheath is a natural laboratory for collisionless plasma turbulence (e.g., Alexandrova et al., 2008; Chen & Boldyrev, 2017; Chhiber et al., 2018; Matteini et al., 2016; Rakhmanova et al., 2021;

Yordanova et al., 2020; Zimbardo et al., 2010), comprised of decelerated, heated, and compressed solar wind plasma which has been deflected around Earth's magnetosphere. Magnetosheath dynamics are influenced by solar wind turbulence as it is processed by the bow shock, as well as fluctuations driven by the shock itself (Huang et al., 2017; Rakhmanova et al., 2021; Sahraoui et al., 2020). In addition to strong fluctuations, the magnetosheath is host to complex velocity distribution functions (VDFs) which deviate significantly from a Maxwellian distribution (Shuster et al., 2019). Like the turbulent fluctuations, the shape of the VDF is influenced by the processing of the shock as well as fluctuations in the magnetosheath. Non-Maxwellian VDFs are susceptible to instabilities, which reduce the free energy in the VDF by scattering particles in velocity space and driving the plasma to relax into a state closer to thermodynamic equilibrium, exciting plasma wave modes (Gary, 1993; Treumann & Baumjohann, 1997).

In collisionless plasmas, internal energy needs to be redistributed via wave—particle interactions, which requires that free energy is used to grow the wave. There are various ways by which free energy can be scattered, but the common factor is that, since magnetic fields ($\mathbf{B}$) cannot do work on particles, energy transfer occurs via interactions with the electric field ($\mathbf{E}$). Energy exchange between the electromagnetic field and bulk flow energy is mediated by $\mathbf{j}\cdot\mathbf{E}$, where $\mathbf{j} = \sum_s q_s n_s \mathbf{v}_s$ is the total current density, q_s is the charge, n_s is the number density, $\mathbf{v}_s$ is the bulk flow velocity, and s denotes the species (Baumjohann & Treumann, 1996). Taking the contribution from the electron-frame electric field $\mathbf{E}' = \mathbf{E} + \mathbf{v}_e \times \mathbf{B}$ gives the Joule dissipation, $\mathbf{j}\cdot\mathbf{E}'$ (Vörös et al., 2019; Zenitani, Hesse, Klimas, Black, & Kuznetsova, 2011), which is the collisionless analogue of Ohmic heating, ηj^2. This term is important for collisionless dissipation (Birn & Hesse, 2005, 2009; Zenitani, Hesse, Klimas, & Kuznetsova, 2011) because it encapsulates energy conversion related to non-ideal electric fields, which are capable of decoupling particle motion from $\mathbf{B}$. In contrast to ηj^2, which is positive by definition, $\mathbf{j}\cdot\mathbf{E}'$ is reversible and therefore sign-indefinite, although space plasma observations typically find it to be positive on average (Matthaeus et al., 2020). Positive values correspond to transfer from fields to flow (loading), whereas negative values correspond to conversion from the flow to the fields (generating) (Birn & Hesse, 2005). Within the magnetosheath, $\mathbf{E}'$ is dominated by $\mathbf{E}_{P_e} = -\frac{1}{n_e e}\nabla\cdot\mathbf{P}_e$ (the pressure term of generalized Ohm's law, where $\mathbf{P}_e$ is the electron pressure tensor and e is the elementary charge) down to the smallest spatial scales which can be sampled by spacecraft instruments (Lewis et al., 2023; Stawarz et al., 2021; Vörös et al., 2019). In the magnetosheath, instrumental resolution is regularly sufficient to sample $\mathbf{E}_{P_e}$ well into the sub-ion range, but rarely below the electron characteristic scales. A key question in the study of collisionless plasma turbulence and its associated dissipation is understanding the origin of both the positive and negative energy conversion signatures and how they may relate to specific fundamental plasma processes.

Prior studies have demonstrated that temperature anisotropy ($T_{s,\perp}/T_{s,\parallel} \neq 1$) is constrained by the parallel plasma beta $\beta_{s,\parallel} = 2n_s k_B T_{s,\parallel}\mu_0/B^2$, where $B = \|\mathbf{B}\|$ is the magnetic field strength, and $T_{s,\parallel}$ and $T_{s,\perp}$ are the temperature parallel and perpendicular to the local $\mathbf{B}$, respectively. Prior studies of the solar wind and magnetosheath have observed this effect for the protons (Bandyopadhyay, Begley, et al., 2022; Gary et al., 1995, 1997; Hellinger et al., 2006; Maruca et al., 2012, 2018; Matteini et al., 2013) and electrons (Gary et al., 2005; Graham et al., 2021; Xu & Chen, 2012; Zhang et al., 2018). The constraint put on $T_{s,\perp}/T_{s,\parallel}$ by $\beta_{s,\parallel}$ is thought to be linked to a number of different instabilities (Gary, 1993), for which empirical functional forms have been developed to parameterize the growth rate contours as a function of dimensionless parameters S_e, α_e (electrons) and a, β_0 (ions). These curves are expressed as $T_{e,\perp}/T_{e,\parallel} = 1 + S_e\,\beta_{e,\parallel}^{-\alpha_e}$ (Gary & Wang, 1996) and $T_{i,\perp}/T_{i,\parallel} = 1 + a\left(\beta_{i,\parallel} - \beta_0\right)^{-b}$ (Hellinger et al., 2006), for the electrons and ions, respectively. When plotted on the anisotropy–beta plane, these curves serve as boundaries of the accessible region of parameter space, indicating that rapidly growing kinetic microinstabilities have a controlling influence on the shape of VDFs. Electron parameter space is bounded by the electron whistler and oblique electron firehose instabilities, whereas the ions are influenced by the ion cyclotron, ion mirror, parallel ion firehose and oblique ion firehose instabilities. In this study, we examine how local anisotropy of the VDF or local $\beta_\parallel$ associated with the turbulent dynamics in the magnetosheath interplay with these kinetic microinstabilities to regulate the energy conversion and dissipation in collisionless plasma turbulence. The instability growth rate thresholds are derived using linear Vlasov theory under the assumption of perturbations to single bi-Maxwellian components for each species growing in a uniform background, in apparent contradiction with the nonlinear, nonuniform conditions characteristic of turbulence. One explanation for how linear theory is applicable in turbulent conditions is that the local nonlinear timescales have been found to be

much slower than linear growth rates in extreme regions of anisotropy–beta parameter space (Bandyopadhyay, Qudsi, et al., 2022). However, this is not always true, especially in the solar wind (Klein et al., 2019a, 2021).

The links between turbulence and small-scale instabilities have recently started to be explored for the protons, for example, in hybrid simulations of Alfvénic turbulence (Bott et al., 2021; Markovskii et al., 2019) and in the solar wind (Opie et al., 2023). However, this is still an open problem. The resonant interactions responsible for particle energization have been the subject of detailed studies in recent years (e.g., Afshari et al., 2021; Chen et al., 2019; Howes et al., 2017; Jiang et al., 2024; Klein et al., 2017; Verniero et al., 2021), however they are difficult to investigate statistically because of their purely kinetic nature and how complex it is to look at individual features in the VDF. Instead, we adopt a fluid approach using $\mathbf{j} \cdot \mathbf{E}'$ to assess the net transfer of energy to and from the particles, neglecting how the dissipation takes place in detail on a particle-by-particle basis. In this letter, we look for the first time at how this fluid heating step is organized with respect to the plasma microinstabilities, to highlight how turbulent fluctuations are interacting with the VDFs to create conditions which are locally susceptible to the kinetic microinstabilities which regulate the plasma thermodynamics.

2. Data

Magnetospheric Multiscale (MMS) (Burch et al., 2016) is a multi-spacecraft mission launched in 2015 to study magnetic reconnection in the geospace environment (Fuselier et al., 2016; Tooley et al., 2016). The mission features four probes orbiting in a tetrahedral formation, containing identical instrument suites which measure electromagnetic fields (Ergun et al., 2016; Lindqvist et al., 2016; Russell et al., 2016; Torbert et al., 2016) and VDFs (Pollock et al., 2016) with unprecedented measurement cadence. In its highest-resolution "burst"-mode, MMS samples the electromagnetic field at up to 8,192 Hz and measures electron and ion VDFs at cadences of 0.03 and 0.15 s respectively. These rapid particle measurements facilitate in-depth exploration of sub-ion scale turbulence that was not possible with prior missions.

Our data set consists of 24.4 hr of single-spacecraft burst-mode data from 163 intervals of continuous magnetosheath measurements by MMS1. The interval list is derived from that used by Stawarz et al. (2022), with additions up until the end of the 2019–2020 MMS dayside season. The intervals, which are tabulated in a CSV file provided in Supporting Information S1, range from 3 to 43 min in length, with a mean of 9 min. There are no large-scale inhomogeneities and all are long enough to cover multiple correlation lengths (the largest scale of turbulent fluctuations). Intervals are aggregated to create a single time series of variables on the electron and ion measurement cadence, as appropriate. Moments of the VDFs are used to compute $\mathbf{j} = en_e(\mathbf{v}_i - \mathbf{v}_e)$ where quasineutrality is used, and $\mathbf{v}_i$ is interpolated onto the electron timescale, since small-scale fluctuations in $\mathbf{j}$ are dominated by $\mathbf{v}_e$ (Stawarz et al., 2021). $\mathbf{E}'$ is calculated on the electron instrument cadence, which requires averaging $\mathbf{E}$ and $\mathbf{B}$ onto the same timescale as $\mathbf{j}$. Instantaneous local values of $\beta_{s,\parallel}$ and $T_{s,\perp}/T_{s,\parallel}$ are used, where the ion values are interpolated onto the electron cadence under the assumption that small-scale fluctuations in these parameters can be neglected. Research in the present study is conducted using measurements at the electron instrument cadence (0.03 s). We have also examined the impact of performing the analysis on data downsampled onto the ion cadence (0.15 s), finding that our results are qualitatively similar.

Figure 1 panels (a) and (b) show how microinstabilities constrain accessible regions of anisotropy–beta parameter space in our data set. Electron and ion instability thresholds are plotted using the parametric curves defined in Gary and Nishimura (2003) and Maruca et al. (2018), respectively, wherein it is assumed that VDFs are anisotropic Maxwellians and that there is no anisotropy for one species when computing the growth curves of the other. Despite nonzero background non-Maxwellianity and correlation between $T_{e,\perp}/T_{e,\parallel}$ and $T_{i,\perp}/T_{i,\parallel}$ within our data set, the plots in Figure 1 demonstrate that the vast majority of probability density lies within instability growth rate thresholds of $\gamma = 10^{-2}\ \Omega_c$, as seen in previous studies (Graham et al., 2021; Maruca et al., 2018). Comparing Figures 1a and 1b, the ions are typically able to deviate further from their respective instability growth rate curves, and crucially the ion probability density appears more diffuse across parameter space, irrespective of instability thresholds. In both panels, the greatest occupancy of parameter space is concentrated around $T_\perp/T_\parallel \sim 1$ and $\beta_\parallel \sim 10^{-1}$–$10^{1}$, indicating the typical conditions in the magnetosheath. Panels (c) to (e) show that turbulent fluctuations generate local changes to both anisotropy and instability thresholds such that the plasma is locally driven closer or farther from the unstable regions, indicating that a typical interval moves significantly around parameter space as opposed to filling an isolated region close to its average. To highlight this, an animation

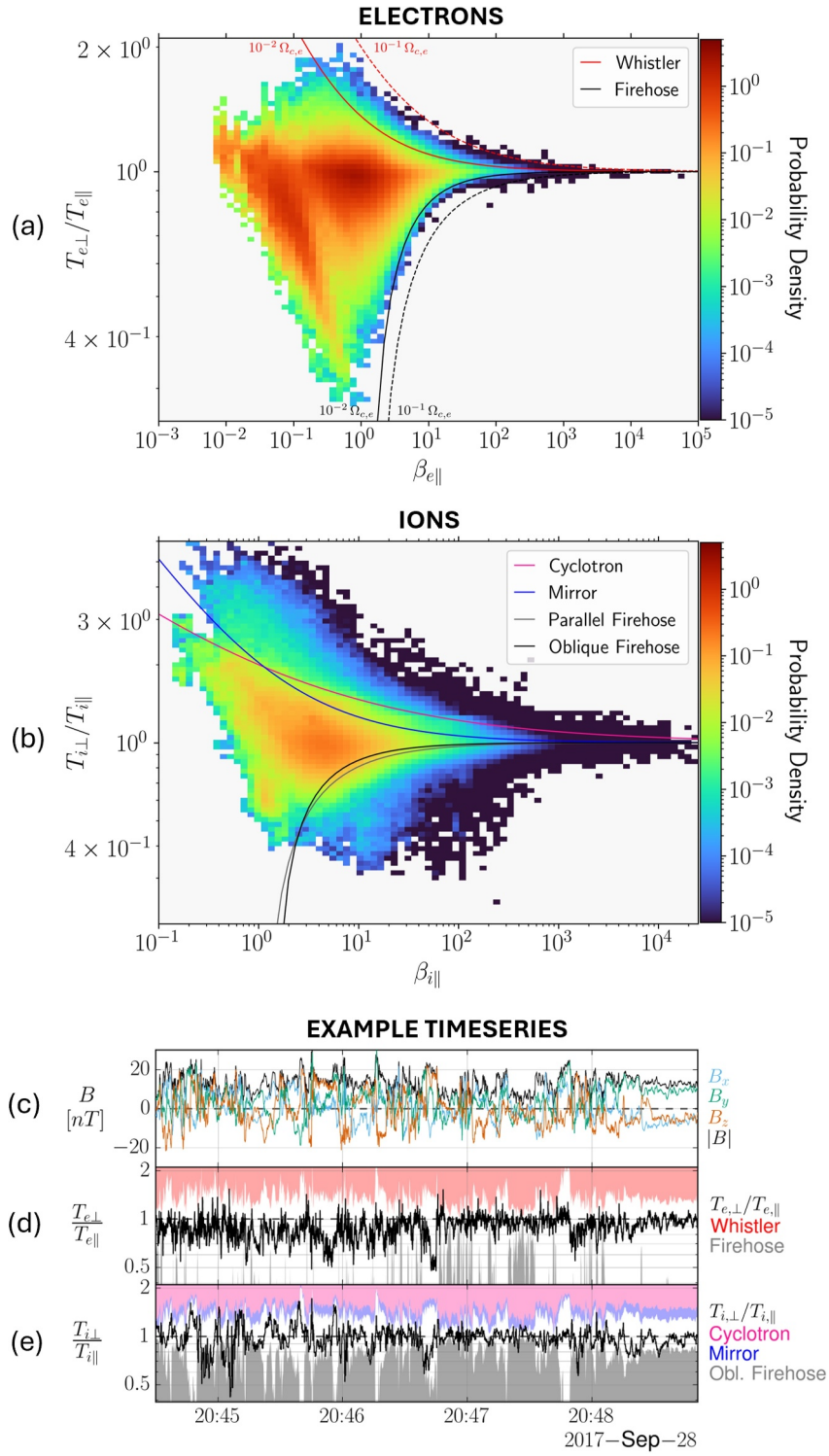

Figure 1. Probability density plotted on the anisotropy–beta plane for our MMS data set, with an example time series. Panel (a) represents the electron plane, where solid and dashed lines correspond to $\gamma = 10^{-2}\ \Omega_{c,e}$ and $\gamma = 10^{-1}\ \Omega_{c,e}$ growth rate thresholds, respectively. Panel (b) shows the ion plane, with $\gamma = 10^{-2}\ \Omega_{c,i}$ instability thresholds. Panels (c)–(e) illustrate motion through parameter space during 2017-09-28/20:44:30-20:48:51. Panel (c) shows the turbulent magnetic field. Panels (d) and (e) show the temperature anisotropy of the electrons and ions, respectively. Shaded areas represent instantaneous $\gamma = 10^{-2}\ \Omega_c$ instability thresholds for each species.

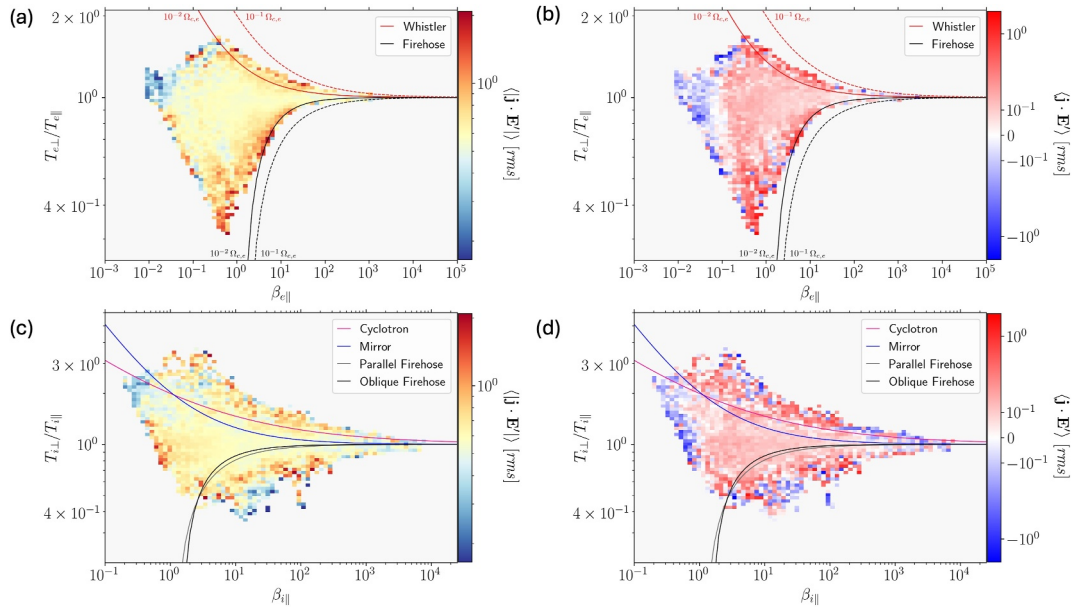

Figure 2. Average amplitude of energy conversion signals distributed on anisotropy–beta plane. (a) $\langle |\mathbf{j}\cdot\mathbf{E}'| \rangle$ in $T_{e,\perp}/T_{e,\parallel}$–$\beta_{e,\parallel}$ parameter space with instability thresholds of $\gamma = 10^{-2}\ \Omega_{c,e}$ (solid line) and $\gamma = 10^{-1}\ \Omega_{c,e}$ (dashed line). (b) $\langle \mathbf{j}\cdot\mathbf{E}' \rangle$ on the same plane. (c) $\langle |\mathbf{j}\cdot\mathbf{E}'| \rangle$ in $T_{i,\perp}/T_{i,\parallel}$–$\beta_{i,\parallel}$ parameter space with instability thresholds of $\gamma = 10^{-2}\ \Omega_{c,i}$. (d) $\langle \mathbf{j}\cdot\mathbf{E}' \rangle$ on the same plane. In all panels, bins with fewer than nine points in total or originating from fewer than two intervals are excluded.

illustrating the trajectory of the example time series through anisotropy—beta space is provided in Supporting Information S1.

3. Results

We investigate how energy conversion to/from the electromagnetic fields is organized with respect to kinetic microinstabilities by plotting $\langle |\mathbf{j}\cdot\mathbf{E}'| \rangle$ and $\langle \mathbf{j}\cdot\mathbf{E}' \rangle$ on the anisotropy–beta plane. To account for any large-scale variability between intervals, we normalize the time series of $\mathbf{j}\cdot\mathbf{E}'$ by its mean-removed root mean square (rms) $= \sqrt{\langle (\mathbf{j}(t)\cdot\mathbf{E}'(t) - \langle \mathbf{j}(t)\cdot\mathbf{E}'(t) \rangle)^2 \rangle}$ on an interval-by-interval basis. The data in these units represents an energy conversion fluctuation where a value of 1 corresponds to the characteristic fluctuation amplitude for the interval from which a given data point originates. Similar qualitative results are obtained based on unnormalized values of $\mathbf{j}\cdot\mathbf{E}'$.

Figure 2a shows that there is enhanced $\langle |\mathbf{j}\cdot\mathbf{E}'| \rangle$—corresponding to a greater mean amplitude of energy conversion signals—in regions susceptible to (oblique) electron firehose and electron whistler instabilities. Qualitatively, high $\langle |\mathbf{j}\cdot\mathbf{E}'| \rangle$ is most strongly concentrated around the firehose threshold, extending to $\gamma \leq 10^{-2}\ \Omega_{c,e}$. In comparison, the enhancement associated with the whistler instability begins at $\gamma \geq 10^{-2}\ \Omega_{c,e}$. Interestingly, there is an enhancement along the low–$\beta_{e,\parallel}$ edge of the distribution for $T_{e,\parallel} > T_{e,\perp}$. Despite being partially obscured in the full set of intervals, closer investigation revealed that this feature is robustly present for different subsets of intervals. Given that this signature is not in the vicinity of the standard instability thresholds, the significance of enhanced $\langle |\mathbf{j}\cdot\mathbf{E}'| \rangle$ in this region of parameter space is less clear. It could be related to a possible instrumental bias shifting the PDF in anisotropy–beta space, but to determine this would require a separate systematic study. Figure 2b shows that mean signed energy conversion is positive across most of parameter space, and that it is particularly strong near the firehose and whistler instability thresholds. The center of the distribution is weakly net-positive, accounting for the majority of overall energy conversion and suggesting that there is an average dissipation of electromagnetic energy into particle energization. At low–$\beta_{e,\parallel}$, there are regions of negative average energy conversion which partially overlap with enhancements in $\langle |\mathbf{j}\cdot\mathbf{E}'| \rangle$.

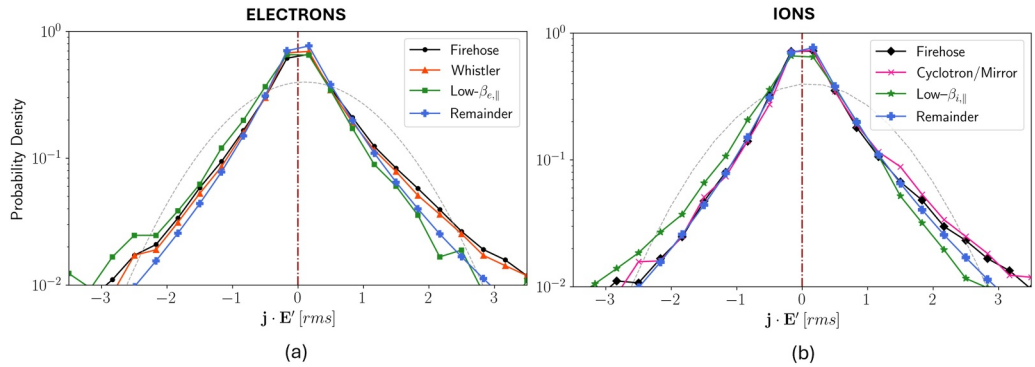

Figure 3. Probability density function of $\mathbf{j} \cdot \mathbf{E}'$ in each region for (a) the electrons and (b) the ions. Markers represent the center of histogram bins. The dashed gray curve indicates a normal distribution with the same mean and standard deviation as the entire data set.

There are interesting comparisons to draw with how energy conversion is organized across ion parameter space. Figure 2c shows that, as for electrons, $\langle|\mathbf{j} \cdot \mathbf{E}'|\rangle$ is enhanced along instability boundaries. However, the enhancement is most pronounced beyond the instability thresholds, suggesting that a faster growth rate is required to overcome the effects which are driving the ion VDFs into unstable regions. An enhancement on the low–$\beta_{i,\parallel}$ edge is also visible, albeit partially obscured as in the electron plot. This similarity may be expected because the time steps that are at $\beta < 1$ are mainly driven by large magnetic fields, appearing as low–$\beta_{\parallel}$ points on both species' planes. Figure 2d shows that $\langle \mathbf{j} \cdot \mathbf{E}' \rangle$ in ion parameter space is more sign-indefinite than the electrons beyond the instability thresholds, with average net conversion from fields to flow only being maintained in the stable center of the distribution.

To investigate the statistical trends identified in anisotropy–beta parameter space, we manually select and group bins into regions of apparent enhanced $\langle|\mathbf{j} \cdot \mathbf{E}'|\rangle$ and investigate their properties. Certain regions have unclear boundaries (particularly those in ion parameter space), which introduces some variability, however the main features we highlight are not impacted by this. Note that the enhancements associated with the ion cyclotron and ion mirror instabilities have been treated as a single region. Figure 3 shows the probability density function (PDF) in each manually defined region for bins in the range $[-3.5, 3.5]$ rms units, within which the vast majority (98.10%) of points lie. For context, 54.77% of the data set has $\mathbf{j} \cdot \mathbf{E}' > 0$ rms units, but only 10.10% has $\mathbf{j} \cdot \mathbf{E}' \geq 1$ rms units and 6.58% has $\mathbf{j} \cdot \mathbf{E}' \leq -1$ rms units. All regions, including the remainders, have nonzero skewness and high kurtosis. Panel (a) shows there is a slight enhancement in the negative tails of the electron PDF relative to the remainder, but a more significant enhancement on the positive side, leading to net positive $\mathbf{j} \cdot \mathbf{E}'$. The low–$\beta_{e,\parallel}$ region has diminished positive tail, but the heaviest negative tail of all the regions. Bins with $|\mathbf{j} \cdot \mathbf{E}'| \gtrsim 2$ rms units do not have enough counts to discern a reliable trend. Panel (b) demonstrates that ion instability regions are nearly identical to the remainder in the negative tail, but are enhanced on the positive side. The low–$\beta_{i,\parallel}$ region is reminiscent of its electron counterpart because they largely share similar points; the negative tails are heavier than positive, and the peak value is smaller. These trends will be assessed quantitatively in the next section.

4. Discussion

There are a number of processes involving energy conversion which may be related to kinetic microinstabilities. Turbulent fluctuations locally driving the plasma toward an instability threshold by distorting the distribution would be expected to give a positive signature. Growth of wave modes as a result of instabilities might be expected to give a negative signature. Redistribution of free energy in velocity space due to wave growth may not show up in $\mathbf{j} \cdot \mathbf{E}'$. In our data set, the presence of strong fluctuations in $\mathbf{j} \cdot \mathbf{E}'$ along the unstable boundaries of the distribution is indicative of a link between turbulence and the underlying instability processes. Largely positive $\langle \mathbf{j} \cdot \mathbf{E}' \rangle$ across parameter space indicates that we predominantly observe the extraction of energy from turbulent fluctuations into the fluid flow. However, around the instability thresholds we see a mixture of net-positive and net-negative bins, particularly for the ions, which suggests we are also sampling part of wave growth due to instabilities.

Table 1
Mean Net and Amplitude of $\boldsymbol{j}\cdot\boldsymbol{E}'$, Variance, Skewness, and Kurtosis by Region

Region	Data (%)	$\langle \mathbf{j}\cdot\mathbf{E}'\rangle$	$\langle \lvert\mathbf{j}\cdot\mathbf{E}'\rvert\rangle$	Variance	Skewness	Kurtosis
Electron firehose	2.48	0.159	0.779	2.00	3.01	79.20
Electron whistler	0.56	0.150	0.721	1.76	5.25	164.99
Electron low–$\beta_{e,\parallel}$	0.14	−0.059	0.755	3.15	−15.96	648.70
Electron remainder	96.82	0.104	0.583	0.97	1.89	94.50
Ion firehose	0.54	0.127	0.683	1.67	2.92	61.60
Ion cyclotron/mirror	0.44	0.155	0.713	2.23	5.55	224.16
Ion low–$\beta_{i,\parallel}$	0.67	−0.040	0.667	1.79	−1.33	824.73
Ion remainder	98.35	0.106	0.587	0.99	2.09	85.51

Table 1 gives the average values of $\mathbf{j}\cdot\mathbf{E}'$ and $|\mathbf{j}\cdot\mathbf{E}'|$ in each manually defined region as introduced in Section 3. The three electron regions represent 3.18% of the total data set, including 3.04% associated with the electron firehose and whistler instabilities. $\langle\mathbf{j}\cdot\mathbf{E}'\rangle$ in the electron instability regions shows that the average energy conversion direction is from the fields to the fluid flow, and that the average value is increased compared to the remainder. This is consistent with electron VDFs being driven into unstable configurations by fluid heating associated with turbulent fluctuations. The low–$\beta_{e,\parallel}$ region has net energy conversion from the fluid flow into the fields, which suggests we are observing the scattering of particles leading to the reduction of free energy in the VDF in favor of growing wave modes. The fraction of data associated with ion regions is lower at 1.65%, with only 0.98% of measurements associated with enhancements in $\mathbf{j}\cdot\mathbf{E}'$ at the ion cyclotron and firehose instabilities. $\langle\mathbf{j}\cdot\mathbf{E}'\rangle$ in the ion regions is similar to electron regions, with net positive energy conversion along instability thresholds and net negative conversion at small $\beta_{i,\parallel}$.

Investigating the average amplitude of signals tells us about how much energy conversion is occurring regardless of direction, without positive and negative values canceling each other out. The electron firehose region has the strongest $\langle|\mathbf{j}\cdot\mathbf{E}'|\rangle$ enhancement, with a 33.6% increase compared to the remainder of the data. The electron whistler region has the smallest increase at 23.6%, but this is still larger than the enhancement in any of the ion regions. The low–$\beta_{e,\parallel}$ region has a 29.5% increase, showing that more energy conversion is occurring on average in this region than in the remainder, albeit on average from flow to fields. Compared to the remainder, the ion instability regions have enhanced $\langle|\mathbf{j}\cdot\mathbf{E}'|\rangle$, by 16.4% (ion firehose) and 21% (ion cyclotron), indicating that smaller energy conversion signatures are present around ion instability thresholds than at equivalent electron boundaries. This implies that energy conversion fluctuations to and from the ion VDFs are on average weaker where kinetic microinstabilities are growing or acting compared to the electron case, possibly as a result of the ions being more nonthermal due to their lower thermal velocity. Similarly to the electron equivalent, the low–$\beta_{i,\parallel}$ region has negative $\langle\mathbf{j}\cdot\mathbf{E}'\rangle$ and increased $\langle|\mathbf{j}\cdot\mathbf{E}'|\rangle$.

For electrons, MMS may not sample particle distributions fast enough to resolve all dynamics. This, and clear net positive $\langle\mathbf{j}\cdot\mathbf{E}'\rangle$, suggests we are preferentially observing the driving of electron VDFs into unstable regions. In contrast, ion dynamics take place on longer timescales, potentially indicating why we can observe fluctuations more clearly, explaining why $\langle|\mathbf{j}\cdot\mathbf{E}'|\rangle$ is enhanced but $\langle\mathbf{j}\cdot\mathbf{E}'\rangle$ is more sign-indefinite in unstable regions. Wave propagation may bias our statistics against observing negative $\mathbf{j}\cdot\mathbf{E}'$ in the electrons, as Svenningsson et al. (2022) found most electron whistler waves are observed away from their source region. Other instabilities may be the same, although the non-propagating electron firehose mode is expected to dominate compared to the propagating mode (Cozzani et al., 2023). However, waves resulting directly from ion instabilities have been observed in the solar wind (Gary et al., 2016; McManus et al., 2024). Additionally, due to Taylor's hypothesis (Taylor, 1938), which is frequently applied to the magnetosheath (and verified to be true for a subset of our intervals in Stawarz et al. (2022)), MMS generally observes spatial slices due to plasma advection rather than temporal slices due to evolution. To account for these effects, a simulation study into $\mathbf{j}\cdot\mathbf{E}'$ and kinetic microinstabilities would be valuable to track how the instability cycle is linked to turbulence as plasma evolves through the magnetosheath.

In this study, we focus on $\mathbf{j}\cdot\mathbf{E}'$ as the representation of non-ideal energy conversion between the electromagnetic fields and particle energy. However, this mechanism is not the only pathway toward dissipation

(Matthaeus et al., 2020; Pezzi et al., 2021). In the statistical formulation of energy transfer channels, the pressure–strain interaction, $-(\mathbf{P}_s \cdot \nabla) \cdot \mathbf{v}_s$, encapsulates energy transfer between fluid flow and random thermal motion (Chasapis et al., 2018; Yang, Matthaeus, Parashar, Haggerty, et al., 2017; Yang, Matthaeus, Parashar, Wu, et al., 2017). Since the collisionless energy transfer quantities are sign-indefinite yet are expected to lead to net dissipation on average, it would be interesting to understand how $\mathbf{j}_s \cdot \mathbf{E}$ and $-(\mathbf{P}_s \cdot \nabla) \cdot \mathbf{v}_s$ balance locally. However, $-(\mathbf{P}_s \cdot \nabla) \cdot \mathbf{v}_s$ is a difficult quantity to compute using observational data because the electron-scale pressure gradients are frequently smaller than can be measured by particle instruments (Dahani et al., 2024).

One process which may be playing a key role in the local distortion of VDFs and excitation of kinetic microinstabilities is turbulence-driven magnetic reconnection, which has recently been attracting significant attention in the magnetosheath. Prior studies have demonstrated that turbulence-driven reconnection events are actively occurring throughout the magnetosheath (e.g., Gingell et al., 2019; Phan et al., 2018; Retino et al., 2007; Sundkvist et al., 2007; Wang et al., 2019), including within some of our intervals (Stawarz et al., 2022). Collisionless magnetic reconnection is well known to generate VDF anisotropy in the outflows and along the separatrices (Egedal et al., 2013), which potentially contributes to driving the distribution in the magnetosheath toward the instability boundaries. In fact, observations of magnetic reconnection in other contexts have clearly demonstrated the generation of firehose fluctuations through this mechanism (Cozzani et al., 2023). Other examples of processes which can modify the internal energy are the divergence of the vector heat flux density (Du et al., 2020), and dissipation associated with an increase in entropy due to collisions (Argall et al., 2022; Barbhuiya et al., 2024; Liang et al., 2019, 2020). Even in weakly collisional plasmas, non-Maxwellian features in the VDF are subject to intraspecies collisions as a result of the dissipation of strong velocity-space gradients (e.g., Pezzi et al., 2021; Schekochihin et al., 2009). Such entropy studies may provide a novel way of assessing the scattering of particles in the VDF associated with the instabilities. Further studies may utilize future spacecraft missions or simulations to expand on the results we have presented here and investigate the links between different energy conversion measures in the context of local turbulence-driven distortions to the VDFs which may be giving rise to kinetic microinstabilities.

5. Conclusion

In this letter, we present a statistical investigation into non-ideal energy conversion associated with kinetic microinstabilities, revealing enhanced levels of $\mathbf{j} \cdot \mathbf{E}'$ close to temperature anisotropy–beta instability thresholds. In these regions, compared to the remainder of the distribution, energy conversion has increased amplitude and larger positive net value, indicating that we more often observe driving of VDFs into unstable configurations than redistribution of free energy in the VDF via scattering of particles and the subsequent growth of wave modes. We find that the greatest enhancement in $\langle \mathbf{j} \cdot \mathbf{E}' \rangle$ and $\langle |\mathbf{j} \cdot \mathbf{E}'| \rangle$ occurs around the electron firehose instability boundary. In contrast, the largest increase in ion parameter space occurs beyond the ion cyclotron instability threshold. We also highlight an additional region of interest, present in both parameter spaces, along the low–$\beta_{\parallel}$ edge, at $T_{e,\perp}/T_{e,\parallel} < 1$ for the electrons and $T_{i,\perp}/T_{i,\parallel} \sim 1$ for the ions. For both species, the low–$\beta_{\parallel}$ edge has net negative energy conversion (with a smaller absolute value than the net of the remainder), highlighting these regions as areas where significant energy is being imparted into electromagnetic activity. The origin of this effect is not yet understood. Despite accounting for a small percentage of the overall observations, we have shown that non-ideal energy conversion is enhanced when VDFs are configured such that they are susceptible to anisotropy-driven kinetic microinstabilities. We suggest that, while these processes are not responsible for the large-scale energy budget of the magnetosheath, the instability growth—excitation—scattering cycle is playing an important active role in how turbulent fluctuations influence the plasma thermodynamics.

There are some unresolved questions which warrant exploration in a further study. The relationship between kinetic microinstabilities and energy conversion parallel and perpendicular to the local **B** is interesting, because of the consequences for particle acceleration along field lines. In addition, there are extra sources of free energy in the VDF arising due to deviations from bi-Maxwellians which are unaccounted for by the anisotropy–beta instability thresholds (Klein et al., 2018, 2019b). Magnetosheath VDFs frequently exist as flat-top distributions with energetic tails (e.g., Formisano et al., 1973), which are related to processing of the solar wind by Earth's bow shock. However, turbulent fluctuations may be playing a role in accelerating non-thermal particles via the turbulent dissipation mechanism (e.g., Bandyopadhyay et al., 2021; Chasapis et al., 2015; Chasapis et al., 2017; Karimabadi et al., 2014; Matthaeus et al., 2015; Wan et al., 2012; Yordanova et al., 2021), contributing to local

enhancements in non-Maxwellianity such as energetic tails. Some work has been done to uncover how non-Maxwellianity is organized with respect to the anisotropy-driven kinetic microinstabilities (Graham et al., 2021; Walters et al., 2023), and future investigations should aim to link trends in the non-Maxwellianity to energy conversion. Finally, other energy conversion measures—such as the pressure–strain interaction, and the contribution to fluid heating from different elements of **j** and various components of **E**—may be treated with a similar analysis as in the present paper in order to uncover their relationship to the regulation of plasma thermodynamics.

Data Availability Statement

The data used in this study are publicly available through the MMS Science Data Center at https://lasp.colorado.edu/mms/sdc/public/. Elements of data analysis were performed using the pyrfu analysis package available at https://github.com/louis-richard/irfu-python.

Acknowledgments
H.C.L. and J.E.S. are supported by the Royal Society University Research Fellowship No. URF\R1\201286. L.F. was supported by the Royal Society University Research Fellowship No. URF\R1\231710 and Science and Technology Facilities council (STFC) Grant ST/W001071/1. H. C.L. and L.F. were supported by the International Exchange Grant IES\R1 \231251. K.G.K. was supported by NASA Grant 80NSSC19K0912. J.H.W. was supported by STFC studentship ST/ X508433/1. Work at UC Berkeley is supported by NASA Grants 80NSSC20K0708 and 80NSSC21K1692. This research was supported by the International Space Science Institute (ISSI) in Bern, through ISSI International Team project #556 (Cross-scale energy transfer in space plasmas). J.E.S. acknowledges useful discussions as part of the ISSI International Team project #588 (Unveiling Energy Conversion and Dissipation in Non-Equilibrium Space Plasmas). The authors wish to thank the entire MMS Team for their work on the mission. H.C.L. thanks colleagues at Imperial College London for valuable discussions.

References

Adhikari, L., Zank, G. P., & Zhao, L. (2021). The transport and evolution of MHD turbulence throughout the Heliosphere: Models and observations. *Fluid*, *6*(10), 368. https://doi.org/10.3390/fluids6100368

Afshari, A. S., Howes, G. G., Kletzing, C. A., Hartley, D. P., & Boardsen, S. A. (2021). The importance of electron Landau damping for the dissipation of turbulent energy in terrestrial magnetosheath plasma. *Journal of Geophysical Research: Space Physics*, *126*(12), e2021JA029578. https://doi.org/10.1029/2021JA029578

Alexandrova, O., Chen, C. H. K., Sorriso-Valvo, L., Horbury, T. S., & Bale, S. D. (2013). Solar wind turbulence and the role of ion instabilities. *Space Science Reviews*, *178*(2–4), 101–139. https://doi.org/10.1007/s11214-013-0004-8

Alexandrova, O., Lacombe, C., & Mangeney, A. (2008). Spectra and anisotropy of magnetic fluctuations in the Earth's magnetosheath: Cluster observations. *Annales Geophysicae*, *26*(11), 3585–3596. https://doi.org/10.5194/angeo-26-3585-2008

Argall, M. R., Barbhuiya, M. H., Cassak, P. A., Wang, S., Shuster, J., Liang, H., et al. (2022). Theory, observations, and simulations of kinetic entropy in a magnetotail electron diffusion region. *Physics of Plasmas*, *29*(2), 022902. https://doi.org/10.1063/5.0073248

Bandyopadhyay, R., Begley, L. J., Maruca, B. A., McComas, D. J., Szalay, J. R., Allegrini, F., et al. (2022a). Beta-Dependent constraints on ion temperature anisotropy in Jupiter's magnetosheath. *Geophysical Research Letters*, *49*(15), e2022GL098053. https://doi.org/10.1029/2022GL098053

Bandyopadhyay, R., Chasapis, A., Matthaeus, W. H., Parashar, T. N., Haggerty, C. C., Shay, M. A., et al. (2021). Energy dissipation in turbulent reconnection. *Physics of Plasmas*, *28*(11), 112305. https://doi.org/10.1063/5.0071015

Bandyopadhyay, R., Qudsi, R. A., Gary, S. P., Matthaeus, W. H., Parashar, T. N., Maruca, B. A., et al. (2022b). Interplay of turbulence and proton-microinstability growth in space plasmas. *Physics of Plasmas*, *29*(10), 102107. https://doi.org/10.1063/5.0098625

Barbhuiya, M. H., Cassak, P. A., Adhikari, S., Parashar, T. N., Liang, H., & Argall, M. R. (2024). Higher-order nonequilibrium term: Effective power density quantifying evolution towards or away from local thermodynamic equilibrium. *Physical Review*, *109*(1), 015205. https://doi.org/10.1103/PhysRevE.109.015205

Baumjohann, W., & Treumann, R. A. (1996). *Basic space plasma physics*. Imperial College Press. https://doi.org/10.1142/p015

Birn, J., & Hesse, M. (2005). Energy release and conversion by reconnection in the magnetotail. *Annales Geophysicae*, *23*(10), 3365–3373. https://doi.org/10.5194/angeo-23-3365-2005

Birn, J., & Hesse, M. (2009). Reconnection in substorms and solar flares: Analogies and differences. *Annales Geophysicae*, *27*(3), 1067–1078. https://doi.org/10.5194/angeo-27-1067-2009

Bott, A. F. A., Arzamasskiy, L., Kunz, M. W., Quataert, E., & Squire, J. (2021). Adaptive critical balance and firehose instability in an expanding, turbulent, collisionless plasma. *The Astrophysical Journal Letters*, *922*(2), L35. https://doi.org/10.3847/2041-8213/ac37c2

Bruno, R., & Carbone, V. (2013). The solar wind as a turbulence laboratory. *Living Reviews in Solar Physics*, *10*(1), 2. https://doi.org/10.12942/lrsp-2013-2

Burch, J. L., Moore, T. E., Torbert, R. B., & Giles, B. L. (2016). Magnetospheric multiscale overview and science objectives. *Space Science Reviews*, *199*(1–4), 5–21. https://doi.org/10.1007/s11214-015-0164-9

Carbone, V. (2012). Scalings, cascade and intermittency in solar wind turbulence. *Space Science Reviews*, *172*(1–4), 343–360. https://doi.org/10.1007/s11214-012-9907-z

Chasapis, A., Matthaeus, W. H., Parashar, T. N., Fuselier, S. A., Maruca, B. A., Phan, T. D., et al. (2017). High-resolution statistics of solar wind turbulence at kinetic scales using the magnetospheric multiscale mission. *The Astrophysical Journal Letters*, *844*(1), L9. https://doi.org/10.3847/2041-8213/aa7ddd

Chasapis, A., Retinó, A., Sahraoui, F., Vaivads, A., Khotyaintsev, Y. V., Sundkvist, D., et al. (2015). Thin current sheets and associated electron heating in turbulent space plasma. *The Astrophysical Journal*, *804*(1), L1. https://doi.org/10.1088/2041-8205/804/1/L1

Chasapis, A., Yang, Y., Matthaeus, W. H., Parashar, T. N., Haggerty, C. C., Burch, J. L., et al. (2018). Energy conversion and collisionless plasma dissipation channels in the turbulent magnetosheath observed by the magnetospheric multiscale mission. *The Astrophysical Journal*, *862*(1), 32. https://doi.org/10.3847/1538-4357/aac775

Chen, C. H. K. (2016). Recent progress in astrophysical plasma turbulence from solar wind observations. *Journal of Plasma Physics*, *82*(6), 535820602. https://doi.org/10.1017/s0022377816001124

Chen, C. H. K., & Boldyrev, S. (2017). Nature of kinetic scale turbulence in the earth's magnetosheath. *The Astrophysical Journal*, *842*(2), 122. https://doi.org/10.3847/1538-4357/aa74e0

Chen, C. H. K., Klein, K. G., & Howes, G. G. (2019). Evidence for electron Landau damping in space plasma turbulence. *Nature Communications*, *10*(1), 740. https://doi.org/10.1038/s41467-019-08435-3

Chhiber, R., Chasapis, A., Bandyopadhyay, R., Parashar, T. N., Matthaeus, W. H., Maruca, B. A., et al. (2018). Higher-order turbulence statistics in the earth's magnetosheath and the solar wind using magnetospheric multiscale observations. *Journal of Geophysical Research: Space Physics*, *123*(12), 9941–9954. https://doi.org/10.1029/2018JA025768

Cozzani, G., Khotyaintsev, Y. V., Graham, D. B., & André, M. (2023). Direct observations of electron firehose fluctuations in the magnetic reconnection outflow. *Journal of Geophysical Research: Space Physics*, *128*(5), e2022JA031128. https://doi.org/10.1029/2022JA031128

Cranmer, S. R., Asgari-Targhi, M., Miralles, M. P., Raymond, J. C., Strachan, L., Tian, H., & Woolsey, L. N. (2015). The role of turbulence in coronal heating and solar wind expansion. *Philosophical Transactions of the Royal Society A: Mathematical, Physical & Engineering Sciences*, *373*(2041), 20140148. https://doi.org/10.1098/rsta.2014.0148

Dahani, S., Lavraud, B., Génot, V., Toledo-Redondo, S., Kieokaew, R., Fargette, N., et al. (2024). Direct in-situ estimates of energy and force balance. In *Near Earth collisionless plasmas*. https://doi.org/10.22541/essoar.171415902.20296148/v1

Du, S., Zank, G. P., Li, X., & Guo, F. (2020). Energy dissipation and entropy in collisionless plasma. *Physical Review*, *101*(3), 033208. https://doi.org/10.1103/PhysRevE.101.033208

Egedal, J., Le, A., & Daughton, W. (2013). A review of pressure anisotropy caused by electron trapping in collisionless plasma, and its implications for magnetic reconnection. *Physics of Plasmas*, *20*(6), 061201. https://doi.org/10.1063/1.4811092

Ergun, R. E., Tucker, S., Westfall, J., Goodrich, K. A., Malaspina, D. M., Summers, D., et al. (2016). The axial double probe and fields signal processing for the MMS mission. *Space Science Reviews*, *199*(1–4), 167–188. https://doi.org/10.1007/s11214-014-0115-x

Evoli, C., & Ferrara, A. (2011). Turbulence in the intergalactic medium: Turbulence in the IGM. *Monthly Notices of the Royal Astronomical Society*, *413*(4), 2721–2734. https://doi.org/10.1111/j.1365-2966.2011.18343.x

Formisano, V., Moreno, G., Palmiotto, F., & Hedgecock, P. C. (1973). Solar wind interaction with the earth's magnetic field: 1. Magnetosheath. *Journal of Geophysical Research*, *78*(19), 3714–3730. https://doi.org/10.1029/JA078i019p03714

Fraternale, F., Adhikari, L., Fichtner, H., Kim, T. K., Kleimann, J., Oughton, S., et al. (2022). Turbulence in the outer heliosphere. *Space Science Reviews*, *218*(6), 50. https://doi.org/10.1007/s11214-022-00914-2

Fuselier, S. A., Lewis, W. S., Schiff, C., Ergun, R., Burch, J. L., Petrinec, S. M., & Trattner, K. J. (2016). Magnetospheric multiscale science mission profile and operations. *Space Science Reviews*, *199*(1–4), 77–103. https://doi.org/10.1007/s11214-014-0087-x

Galtier, S. (2018). Turbulence in space plasmas and beyond. *Journal of Physics A: Mathematical and Theoretical*, *51*(29), 293001. https://doi.org/10.1088/1751-8121/aac4c7

Gary, S. P. (1993). *Theory of space plasma microinstabilities*. (1st ed.). Cambridge University Press. https://doi.org/10.1017/CBO9780511551512

Gary, S. P., Jian, L. K., Broiles, T. W., Stevens, M. L., Podesta, J. J., & Kasper, J. C. (2016). Ion-driven instabilities in the solar wind: Wind observations of 19 March 2005. *Journal of Geophysical Research: Space Physics*, *121*(1), 30–41. https://doi.org/10.1002/2015JA021935

Gary, S. P., Lavraud, B., Thomsen, M. F., Lefebvre, B., & Schwartz, S. J. (2005). Electron anisotropy constraint in the magnetosheath: Cluster observations. *Geophysical Research Letters*, *32*(13), 2005GL023234. https://doi.org/10.1029/2005GL023234

Gary, S. P., & Nishimura, K. (2003). Resonant electron firehose instability: Particle-in-cell simulations. *Physics of Plasmas*, *10*(9), 3571–3576. https://doi.org/10.1063/1.1590982

Gary, S. P., Thomsen, M. F., Yin, L., & Winske, D. (1995). Electromagnetic proton cyclotron instability: Interactions with magnetospheric protons. *Journal of Geophysical Research*, *100*(A11), 21961–21972. https://doi.org/10.1029/95JA01403

Gary, S. P., & Wang, J. (1996). Whistler instability: Electron anisotropy upper bound. *Journal of Geophysical Research*, *101*(A5), 10749–10754. https://doi.org/10.1029/96JA00323

Gary, S. P., Wang, J., Winske, D., & Fuselier, S. A. (1997). Proton temperature anisotropy upper bound. *Journal of Geophysical Research*, *102*(A12), 27159–27169. https://doi.org/10.1029/97JA01726

Gingell, I., Schwartz, S. J., Eastwood, J. P., Burch, J. L., Ergun, R. E., Fuselier, S., et al. (2019). Observations of magnetic reconnection in the transition region of Quasi-parallel shocks. *Geophysical Research Letters*, *46*(3), 1177–1184. https://doi.org/10.1029/2018GL081804

Graham, D. B., Khotyaintsev, Y. V., André, M., Vaivads, A., Chasapis, A., Matthaeus, W. H., et al. (2021). Non-maxwellianity of electron distributions near earth's magnetopause. *Journal of Geophysical Research: Space Physics*, *126*(10). https://doi.org/10.1029/2021JA029260

Guio, P., & Pẽcseli, H. L. (2021). The impact of turbulence on the ionosphere and magnetosphere. *Frontiers in Astronomy and Space Sciences*, *7*, 573746. https://doi.org/10.3389/fspas.2020.573746

Hellinger, P., Trávníček, P., Kasper, J. C., & Lazarus, A. J. (2006). Solar wind proton temperature anisotropy: Linear theory and WIND/SWE observations. *Geophysical Research Letters*, *33*(9), L09101. https://doi.org/10.1029/2006GL025925

Howes, G. G., Klein, K. G., & Li, T. C. (2017). Diagnosing collisionless energy transfer using field-particle correlations: Vlasov-Poisson plasmas. *Journal of Plasma Physics*, *83*(1), 705830102. https://doi.org/10.1017/S0022377816001197

Huang, S. Y., Hadid, L. Z., Sahraoui, F., Yuan, Z. G., & Deng, X. H. (2017). On the existence of the Kolmogorov inertial range in the terrestrial magnetosheath turbulence. *The Astrophysical Journal*, *836*(1), L10. https://doi.org/10.3847/2041-8213/836/1/L10

Jiang, W., Verscharen, D., Jeong, S.-Y., Li, H., Klein, K. G., Owen, C. J., & Wang, C. (2024). Velocity-space signatures of resonant energy transfer between whistler waves and electrons in the earth's magnetosheath. *The Astrophysical Journal*, *960*(1), 30. https://doi.org/10.3847/1538-4357/ad0df8

Karimabadi, H., Roytershteyn, V., Vu, H. X., Omelchenko, Y. A., Scudder, J., Daughton, W., et al. (2014). The link between shocks, turbulence, and magnetic reconnection in collisionless plasmas. *Physics of Plasmas*, *21*(6), 062308. https://doi.org/10.1063/1.4882875

Kiyani, K. H., Osman, K. T., & Chapman, S. C. (2015). Dissipation and heating in solar wind turbulence: From the macro to the micro and back again. *Philosophical Transactions of the Royal Society A: Mathematical, Physical & Engineering Sciences*, *373*(2041), 20140155. https://doi.org/10.1098/rsta.2014.0155

Klein, K. G., Alterman, B., Stevens, M., Vech, D., & Kasper, J. (2018). Majority of solar wind intervals support ion-driven instabilities. *Physical Review Letters*, *120*(20), 205102. https://doi.org/10.1103/PhysRevLett.120.205102

Klein, K. G., Howes, G. G., & TenBarge, J. M. (2017). Diagnosing collisionless energy transfer using field-particle correlations: Gyrokinetic turbulence. *Journal of Plasma Physics*, *83*(4), 535830401. https://doi.org/10.1017/S0022377817000563

Klein, K. G., Martinović, M., Stansby, D., & Horbury, T. S. (2019a). Linear stability in the inner heliosphere: Helios Re-evaluated. *The Astrophysical Journal*, *887*(2), 234. https://doi.org/10.3847/1538-4357/ab5802

Klein, K. G., Martinović, M., Stansby, D., & Horbury, T. S. (2019b). Linear stability in the inner heliosphere: Helios Re-evaluated. *The Astrophysical Journal*, *887*(2), 234. https://doi.org/10.3847/1538-4357/ab5802

Klein, K. G., Verniero, J. L., Alterman, B., Bale, S., Case, A., Kasper, J. C., et al. (2021). Inferred linear stability of Parker solar probe observations using one- and two-component proton distributions. *The Astrophysical Journal*, *909*(1), 7. https://doi.org/10.3847/1538-4357/abd7a0

Lewis, H. C., Stawarz, J. E., Franci, L., Matteini, L., Klein, K., Salem, C. S., et al. (2023). Magnetospheric Multiscale measurements of turbulent electric fields in earth's magnetosheath: How do plasma conditions influence the balance of terms in generalized Ohm's law? *Physics of Plasmas*, *30*(8), 082901. https://doi.org/10.1063/5.0158067

Liang, H., Barbhuiya, M. H., Cassak, P. A., Pezzi, O., Servidio, S., Valentini, F., & Zank, G. P. (2020). Kinetic entropy-based measures of distribution function non-Maxwellianity: Theory and simulations. *Journal of Plasma Physics*, *86*(5), 825860502. https://doi.org/10.1017/S0022377820001270

Liang, H., Cassak, P. A., Servidio, S., Shay, M. A., Drake, J. F., Swisdak, M., et al. (2019). Decomposition of plasma kinetic entropy into position and velocity space and the use of kinetic entropy in particle-in-cell simulations. *Physics of Plasmas*, *26*(8), 082903. https://doi.org/10.1063/1.5098888

Lindqvist, P. A., Olsson, G., Torbert, R. B., King, B., Granoff, M., Rau, D., et al. (2016). The spin-plane double probe electric field instrument for MMS. *Space Science Reviews*, *199*(1–4), 137–165. https://doi.org/10.1007/s11214-014-0116-9

Linsky, J., Redfield, S., Ryder, D., & Moebius, E. (2022). Inhomogeneity in the local ISM and its relation to the heliosphere. *Space Science Reviews*, *218*(3), 16. https://doi.org/10.1007/s11214-022-00884-5

Marino, R., & Sorriso-Valvo, L. (2023). Scaling laws for the energy transfer in space plasma turbulence. *Physics Reports*, *1006*, 1–144. https://doi.org/10.1016/j.physrep.2022.12.001

Markovskii, S. A., Vasquez, B. J., & Chandran, B. D. G. (2019). Proton temperature-anisotropy instability coexisting with ambient turbulence in the solar-wind plasma. *The Astrophysical Journal*, *875*(2), 125. https://doi.org/10.3847/1538-4357/ab0f9d

Maruca, B. A., Chasapis, A., Gary, S. P., Bandyopadhyay, R., Chhiber, R., Parashar, T. N., et al. (2018). *MMS* observations of beta-dependent constraints on ion temperature anisotropy in earth's magnetosheath. *The Astrophysical Journal*, *866*(1), 25. https://doi.org/10.3847/1538-4357/aaddfb

Maruca, B. A., Kasper, J. C., & Gary, S. P. (2012). Instability-driven limits on helium temperature anisotropy in the solar wind: Observations and linear vlasov analysis. *The Astrophysical Journal*, *748*(2), 137. https://doi.org/10.1088/0004-637X/748/2/137

Matteini, L., Alexandrova, O., Chen, C. H. K., & Lacombe, C. (2016). Electric and magnetic spectra from MHD to electron scales in the magnetosheath. *Monthly Notices of the Royal Astronomical Society*, *466*(1), 945–951. https://doi.org/10.1093/mnras/stw3163

Matteini, L., Hellinger, P., Goldstein, B. E., Landi, S., Velli, M., & Neugebauer, M. (2013). Signatures of kinetic instabilities in the solar wind. *Journal of Geophysical Research: Space Physics*, *118*(6), 2771–2782. https://doi.org/10.1002/jgra.50320

Matthaeus, W. H. (2021). Turbulence in space plasmas: Who needs it? *Physics of Plasmas*, *28*(3), 032306. https://doi.org/10.1063/5.0041540

Matthaeus, W. H., & Velli, M. (2011). Who needs turbulence? A review of turbulence effects in the heliosphere and on the fundamental process of reconnection. *Space Science Reviews*, *160*(1–4), 145–168. https://doi.org/10.1007/s11214-011-9793-9

Matthaeus, W. H., Wan, M., Servidio, S., Greco, A., Osman, K. T., Oughton, S., & Dmitruk, P. (2015). Intermittency, nonlinear dynamics and dissipation in the solar wind and astrophysical plasmas. *Philosophical Transactions of the Royal Society A: Mathematical, Physical & Engineering Sciences*, *373*(2041), 20140154. https://doi.org/10.1098/rsta.2014.0154

Matthaeus, W. H., Yang, Y., Wan, M., Parashar, T. N., Bandyopadhyay, R., Chasapis, A., et al. (2020). Pathways to dissipation in weakly collisional plasmas. *The Astrophysical Journal*, *891*(1), 101. https://doi.org/10.3847/1538-4357/ab6d6a

McManus, M. D., Klein, K. G., Bale, S. D., Bowen, T. A., Huang, J., Larson, D., et al. (2024). Proton- and alpha-driven instabilities in an ion cyclotron wave event. *The Astrophysical Journal*, *961*(1), 142. https://doi.org/10.3847/1538-4357/ad05ba

Opie, S., Verscharen, D., Chen, C. H. K., Owen, C. J., & Isenberg, P. A. (2023). The effect of variations in the magnetic field direction from turbulence on kinetic-scale instabilities. *Astronomy and Astrophysics*, *672*, L4. https://doi.org/10.1051/0004-6361/202345965

Pezzi, O., Liang, H., Juno, J. L., Cassak, P. A., Vásconez, C. L., Sorriso-Valvo, L., et al. (2021). Dissipation measures in weakly collisional plasmas. *Monthly Notices of the Royal Astronomical Society*, *505*(4), 4857–4873. https://doi.org/10.1093/mnras/stab1516

Phan, T. D., Eastwood, J. P., Shay, M. A., Drake, J. F., Sonnerup, B. U. Ã., Fujimoto, M., et al. (2018). Electron magnetic reconnection without ion coupling in Earth's turbulent magnetosheath. *Nature*, *557*(7704), 202–206. https://doi.org/10.1038/s41586-018-0091-5

Pollock, C., Moore, T., Jacques, A., Burch, J., Gliese, U., Saito, Y., et al. (2016). Fast plasma investigation for magnetospheric multiscale. *Space Science Reviews*, *199*(1–4), 331–406. https://doi.org/10.1007/s11214-016-0245-4

Rakhmanova, L., Riazantseva, M., & Zastenker, G. (2021). Plasma and magnetic field turbulence in the earth's magnetosheath at ion scales. *Frontiers in Astronomy and Space Sciences*, *7*. https://doi.org/10.3389/fspas.2020.616635

Retinó, A., Sundkvist, D., Vaivads, A., Mozer, F., André, M., & Owen, C. J. (2007). In situ evidence of magnetic reconnection in turbulent plasma. *Nature Physics*, *3*(4), 235–238. https://doi.org/10.1038/nphys574

Russell, C. T., Anderson, B. J., Baumjohann, W., Bromund, K. R., Dearborn, D., Fischer, D., et al. (2016). The magnetospheric multiscale magnetometers. *Space Science Reviews*, *199*(1–4), 189–256. https://doi.org/10.1007/s11214-014-0057-3

Ruszkowski, M., & Pfrommer, C. (2023). Cosmic ray feedback in galaxies and galaxy clusters: A pedagogical introduction and a topical review of the acceleration, transport, observables, and dynamical impact of cosmic rays. *Astronomy and Astrophysics Review*, *31*(1), 4. https://doi.org/10.1007/s00159-023-00149-2

Sahraoui, F., Hadid, L., & Huang, S. (2020). Magnetohydrodynamic and kinetic scale turbulence in the near-earth space plasmas: A (short) biased review. *Reviews of Modern Plasma Physics*, *4*(1), 4. https://doi.org/10.1007/s41614-020-0040-2

Saur, J. (2021). Turbulence in the magnetospheres of the outer planets. *Frontiers in Astronomy and Space Sciences*, *8*, 624602. https://doi.org/10.3389/fspas.2021.624602

Schekochihin, A. A. (2022). MHD turbulence: A biased review. *Journal of Plasma Physics*, *88*(5), 155880501. https://doi.org/10.1017/S0022377822000721

Schekochihin, A. A., Cowley, S. C., Dorland, W., Hammett, G. W., Howes, G. G., Quataert, E., & Tatsuno, T. (2009). Astrophysical gyrokinetics: Kinetic and fluid turbulent cascades in magnetized weakly collisional plasmas. *The Astrophysical Journal - Supplement Series*, *182*(1), 310–377. https://doi.org/10.1088/0067-0049/182/1/310

Shuster, J. R., Gershman, D. J., Chen, L. J., Wang, S., Bessho, N., Dorelli, J. C., et al. (2019). MMS measurements of the vlasov equation: Probing the electron pressure divergence within thin current sheets. *Geophysical Research Letters*, *46*(14), 7862–7872. https://doi.org/10.1029/2019GL083549

Smith, C. W., & Vasquez, B. J. (2021). Driving and dissipation of solar-wind turbulence: What is the evidence? *Frontiers in Astronomy and Space Sciences*, *7*, 611909. https://doi.org/10.3389/fspas.2020.611909

Stawarz, J. E., Eastwood, J. P., Phan, T. D., Gingell, I. L., Pyakurel, P. S., Shay, M. A., et al. (2022). Turbulence-driven magnetic reconnection and the magnetic correlation length: Observations from Magnetospheric Multiscale in Earth's magnetosheath. *Physics of Plasmas*, *29*(1), 012302. https://doi.org/10.1063/5.0071106

Stawarz, J. E., Matteini, L., Parashar, T. N., Franci, L., Eastwood, J. P., Gonzalez, C. A., et al. (2021). Comparative analysis of the various generalized ohm's law terms in magnetosheath turbulence as observed by magnetospheric multiscale. *Journal of Geophysical Research: Space Physics*, *126*(1), 2020JA028447. https://doi.org/10.1029/2020JA028447

Stepanova, M., Borovsky, J. E., Retino, A., Uritsky, V., Vörös, Z., & Zimbardo, G. (2022). Editorial: The role of turbulence in the solar wind, magnetosphere, ionosphere dynamics. *Frontiers in Astronomy and Space Sciences*, *8*, 763190. https://doi.org/10.3389/fspas.2021.763190

Subramanian, K., Shukurov, A., & Haugen, N. E. L. (2006). Evolving turbulence and magnetic fields in galaxy clusters. *Monthly Notices of the Royal Astronomical Society*, *366*(4), 1437–1454. https://doi.org/10.1111/j.1365-2966.2006.09918.x

Sundkvist, D., Retino, A., Vaivads, A., & Bale, S. D. (2007). Dissipation in turbulent plasma due to reconnection in thin current sheets. *Physical Review Letters*, *99*(2), 025004. https://doi.org/10.1103/PhysRevLett.99.025004

Svenningsson, I., Yordanova, E., Cozzani, G., Khotyaintsev, Y. V., & André, M. (2022). Kinetic generation of whistler waves in the turbulent magnetosheath. *Geophysical Research Letters*, *49*(15). https://doi.org/10.1029/2022GL099065

Taylor, G. I. (1938). The spectrum of turbulence. *Proceedings of the Royal Society of London. Series A - Mathematical and Physical Sciences*, *164*(919), 476–490. https://doi.org/10.1098/rspa.1938.0032

Tooley, C. R., Black, R. K., Robertson, B. P., Stone, J. M., Pope, S. E., & Davis, G. T. (2016). The magnetospheric multiscale constellation. *Space Science Reviews*, *199*(1–4), 23–76. https://doi.org/10.1007/s11214-015-0220-5

Torbert, R. B., Russell, C. T., Magnes, W., Ergun, R. E., Lindqvist, P. A., Le Contel, O., et al. (2016). The FIELDS instrument suite on MMS: Scientific objectives, measurements, and data products. *Space Science Reviews*, *199*(1–4), 105–135. https://doi.org/10.1007/s11214-014-0109-8

Treumann, R. A., & Baumjohann, W. (1997). *Advanced space plasma physics*. Imperial College Press. https://doi.org/10.1142/p020

Verniero, J. L., Howes, G. G., Stewart, D. E., & Klein, K. G. (2021). Determining threshold instrumental resolutions for resolving the velocity-space signature of ion Landau damping. *Journal of Geophysical Research: Space Physics*, *126*(5), e2020JA028361. https://doi.org/10.1029/2020JA028361

Verscharen, D., Klein, K. G., & Maruca, B. A. (2019). The multi-scale nature of the solar wind. *Living Reviews in Solar Physics*, *16*(1), 5. https://doi.org/10.1007/s41116-019-0021-0

Vörös, Z., Yordanova, E., Khotyaintsev, Y. V., Varsani, A., & Narita, Y. (2019). Energy conversion at kinetic scales in the turbulent magnetosheath. *Frontiers in Astronomy and Space Sciences*, *6*, 60. https://doi.org/10.3389/fspas.2019.00060

Walters, J., Klein, K. G., Lichko, E., Stevens, M. L., Verscharen, D., & Chandran, B. D. G. (2023). The effects of nonequilibrium velocity distributions on Alfvén ion-cyclotron waves in the solar wind. *The Astrophysical Journal*, *955*(2), 97. https://doi.org/10.3847/1538-4357/acf1fa

Wan, M., Matthaeus, W. H., Karimabadi, H., Roytershteyn, V., Shay, M., Wu, P., et al. (2012). Intermittent dissipation at kinetic scales in collisionless plasma turbulence. *Physical Review Letters*, *109*(19), 195001. https://doi.org/10.1103/PhysRevLett.109.195001

Wang, S., Chen, L., Bessho, N., Hesse, M., Wilson, L. B., Giles, B., et al. (2019). Observational evidence of magnetic reconnection in the terrestrial bow shock transition region. *Geophysical Research Letters*, *46*(2), 562–570. https://doi.org/10.1029/2018GL080944

Xu, D., & Chen, T. (2012). Constraints on electron temperature anisotropies in sheath regions of interplanetary shocks. *Planetary and Space Science*, *62*(1), 100–103. https://doi.org/10.1016/j.pss.2011.12.015

Yang, Y., Matthaeus, W. H., Parashar, T. N., Haggerty, C. C., Roytershteyn, V., Daughton, W., et al. (2017a). Energy transfer, pressure tensor, and heating of kinetic plasma. *Physics of Plasmas*, *24*(7), 072306. https://doi.org/10.1063/1.4990421

Yang, Y., Matthaeus, W. H., Parashar, T. N., Wu, P., Wan, M., Shi, Y., et al. (2017b). Energy transfer channels and turbulence cascade in Vlasov-Maxwell turbulence. *Physical Review*, *95*(6), 061201. https://doi.org/10.1103/PhysRevE.95.061201

Yordanova, E., Vörös, Z., Raptis, S., & Karlsson, T. (2020). Current sheet statistics in the magnetosheath. *Frontiers in Astronomy and Space Sciences*, *7*(2). https://doi.org/10.3389/fspas.2020.00002

Yordanova, E., Vörös, Z., Sorriso-Valvo, L., Dimmock, A. P., & Kilpua, E. (2021). A possible link between turbulence and plasma heating. *The Astrophysical Journal*, *921*(1), 65. https://doi.org/10.3847/1538-4357/ac1942

Zank, G. P., Zhao, L.-L., Adhikari, L., Telloni, D., Kasper, J. C., & Bale, S. D. (2021). Turbulence transport in the solar corona: Theory, modeling, and Parker solar probe. *Physics of Plasmas*, *28*(8), 080501. https://doi.org/10.1063/5.0055692

Zenitani, S., Hesse, M., Klimas, A., Black, C., & Kuznetsova, M. (2011). The inner structure of collisionless magnetic reconnection: The electron-frame dissipation measure and Hall fields. *Physics of Plasmas*, *18*(12), 122108. https://doi.org/10.1063/1.3662430

Zenitani, S., Hesse, M., Klimas, A., & Kuznetsova, M. (2011). New measure of the dissipation region in collisionless magnetic reconnection. *Physical Review Letters*, *106*(19), 195003. https://doi.org/10.1103/PhysRevLett.106.195003

Zhang, X., Angelopoulos, V., Artemyev, A. V., & Liu, J. (2018). Whistler and electron firehose instability control of electron distributions in and around dipolarizing flux bundles. *Geophysical Research Letters*, *45*(18), 9380–9389. https://doi.org/10.1029/2018GL079613

Zimbardo, G., Greco, A., Sorriso-Valvo, L., Perri, S., Vörös, Z., Aburjania, G., et al. (2010). Magnetic turbulence in the geospace environment. *Space Science Reviews*, *156*(1–4), 89–134. https://doi.org/10.1007/s11214-010-9692-5